Bioengineering a cryogel-derived bioartificial liver using particle image velocimetry defined fluid dynamics

Flavia Bonalumi[1], Cyril Crua[2], Irina N. Savina[1], Nathan Davies[3], Abeba Habstesion[3], Maurizio Santini[4], Stephanie Fest-Santini[5], Susan Sandeman[1]

[1] School of Pharmacy and Biomolecular Sciences, University of Brighton, Brighton, United Kingdom
[2] Advanced Engineering Centre, University of Brighton, Brighton, United Kingdom
[3] The Institute for Liver and Digestive Health, University College London, London, United Kingdom
[4] Dipartimento di Ingegneria e Scienze Applicate, Università degli Studi di Bergamo, Bergamo, Italy
[5] Dipartimento di Ingegneria Gestionale, dell'Informazione e della Produzione, Università degli Studi di Bergamo, Bergamo, Italy

Corresponding author details:

email: s.sandeman@brighton.ac.uk

Abstract

Bioartificial Liver (BAL) devices are extracorporeal systems designed to support or recover hepatic function in patients with liver failure. The design of an effective BAL remains an open challenge since it requires a complex co-optimisation of cell colonisation, biomaterial scaffold and BAL fluid dynamics. Building on previous evidence of suitability as a blood perfusion device for detoxification, the current study investigated the use of RGD-containing p(HEMA)-alginate cryogels as BAL scaffolds. Cryogels were modified with alginate to reduce protein fouling and functionalised with an RGD-containing peptide to increase hepatocyte adhesion. A novel approach for characterisation of the internal flow through the porous matrix was developed by employing Particle Image Velocimetry (PIV) to visualise flow inside cryogels. Based on PIV results, which showed the laminar nature of flow inside cryogel pores, a multi-layered bioreactor composed of spaced cryogel discs was designed to improve blood/hepatocyte mass exchange. The stacked bioreactor showed a significantly higher production of albumin and urea compared to the column version, with improved cell colonisation and proliferation over time. The cell-free cryogel-based device was tested for safety in a bile-duct ligation model of liver cirrhosis. Thus, a stacked bioreactor prototype was developed based on a surface-engineered cryogel design with optimised fluid dynamics for BAL use.

Key words: bioartificial liver, cell scaffold, cryogels, alginate, RGD-peptide, µPIV, BDL model

1. Introduction

Liver disease is a condition that currently affects 29 million people in Europe alone [1] and there are still no effective treatments for the most severe forms other than liver transplantation [2]. 14.3% of

patients die whilst on the transplant waiting list [3] and, for this reason, finding innovative and effective treatments remains critical. Bioartificial liver (BAL) devices are extracorporeal systems designed to sustain liver functionality, conjugating both detoxification and metabolic functions through incorporation of a cellular component inside the bioreactor compartment. Fewer than ten BAL prototypes have undergone clinical trials to date [2] and most of them possessed a hollow fibre configuration. In hollow fibre cartridges, hepatocytes are cultured on the external part of the cylindrical fibres whilst the patients' blood or plasma flows inside, exchanging toxins and nutrients through the fibre [4]. The first two BALs clinically tested were the Extracorporeal Liver Assist Device (ELAD) developed by Ellis et al. [5] in 1996, which employed a human hepatocyte cell line C3A seeded onto cellulose acetate-based hollow fibres, and the HepatAssist device developed in 2000 by Detry et al. [6], in which porcine primary hepatocytes were attached to dextran microcarriers coated with collagen. However, to date no clear clinical efficacy has been demonstrated. Failure may be influenced by a lack of critical cell mass and the exposure of the cells to a highly toxic environment. Currently, new BAL configurations are under investigation with different materials and cell sources, for example employing composite fibres in a polysulfone-chitosan matrix [7] or using polypropylene hollow fibres [8] to support HepG2 human hepatocytes. The group of Selden et al. [9] developed a fluidised bed-based bioreactor to house alginate-encapsulated HepG2 spheroids and the group of Chen et al. [10] investigated a spheroid reservoir BAL using porcine primary hepatocytes. Both groups tested the BAL prototypes in pre-clinical studies on large animal models. The group of Hou et al. [11] recently developed a porous chitosan/gelatin scaffold for BAL purpose by a freeze-drying method using glutaraldehyde as cross-linker. They obtained scaffolds with increasing porosity by decreasing the amount of glutaraldehyde used. However, the smaller amount of glutaraldehyde used to cross-link resulted in an acceleration of the degradation rate, which is not desirable for BAL systems. Whilst these new studies showed promising preliminary results, they have yet to reach clinical trial. The ideal BAL should support a viable cell fraction of approximately 20% of functional cell mass (10^{10} cells) within the normal liver and have adequate mechanical properties to support flow perfusion [12]. It should also maximise mass exchange between patient blood and cells with optimised fluid dynamics to prevent cell damage, provide sufficient oxygenation, nutrient supply and waste removal. Furthermore, the scaffold should be biocompatible to prevent blood cell activation and an inflammatory response.

In this work we have exploited cryogels for BAL design, as cryogels offer a cell supporting environment, mechanical strength and good permeability suitable for the design of a flow perfusion device. Cryogels are supermacroporous hydrogels, which can be produced with a pore size of up to 200 μm and an interconnected network of pores. This interconnecting internal porous network is obtained by

cryogelation; a technique which exploits the crystallisation of a solvent when the temperature is dropped below its freezing point [13-15]. In the last decade cryogels have been used for a variety of applications such as bioseparation, biocatalysis, chromatography and toxin removal [16-18]. These macroporous matrices are promising materials for use as cell scaffolds in tissue engineering, since a pore size between 100 and 300 μm is needed to provide the necessary 3D architecture, organisation of cells and waste removal [19]. Several studies in the past few years focused on cellular colonisation of porous cryogels for organ regeneration. For example, cryogels linked to laminin were employed successfully to differentiate stem cells into neural tissue [20], while softer cryogels made of agarose and p(HEMA)-gelatin were used to culture pancreatic islets [21] and myoblast skeletal cells [22] respectively. Gelatin-fibrinogen and chitosan cryogels have also shown promise in wound dressing applications [23-25]. The open macroporosity, the interconnectivity of the pore network and the mechanical properties make cryogels also good candidates for use in a fluid-perfused device. For example, Berillo et al. [26] built a cryogel-based bioreactor with direct cross-linking of active bacteria to biodegrade phenol derivatives for water treatment and Ingavle et al. [27] successfully synthesised antibody bound acrylate and methacrylate based cryogels for use in a perfused device for blood detoxification to treat life-threatening infection. In addition, cryogels can be freeze dried with shape memory characteristics for ease of storage and use

Cryogels for BAL application have been investigated by Jain et al. [28, 29] who developed a monolith column prototype using an interpenetrating polymer network (IPN) of chitosan and poly(N-isopropylacrylamide) (poly(NiPAA) cryogel as a cell scaffold for HepG2. Some slight improvement in liver function, measured by albumin and urea production and ammonia detoxification, was observed for up to 3 hours when plasma from alcoholic ALF patients was recirculated, after which hepatocyte function declined possibly due to exposure to plasma toxins, hypoxia and hypoglycaemia. The material also absorbed 90% of the serum proteins and 20% BSA, which may lead to a non-specific adsorption of biomolecules from plasma, promoting blood cell activation and inflammation. In a further study [30] the poly(NiPAA) cryogel was modified with a decellularized liver matrix from rat to mimic the ECM surface properties. Although the coating slightly improved HepgG2 proliferation and functionality, the process to decellularize rat liver is expensive in terms of time and cost and can potentially elicit an immune response.

Dynamic flow parameters are an important aspect for maintaining hepatocyte viability and metabolic activity in two-dimensional (2D) systems. The group of Kan et al. [31] found that hepatocytes produced urea and detoxified ammonia when cultured under dynamic flow but not under static conditions, and

only when shear stress did not reach harmful levels. Subsequent studies on 2D and 3D dynamic hepatocyte cultures confirmed this finding [32-34]. Despite the known importance of flow shear stress on cell viability and inflammation pathways, most of the studies on the matter are *in silico* simulations based on micro-CT reconstruction [35-37] and mathematical models [38]. There are currently limited direct experimental investigations of fluid dynamics inside 3D scaffolds for perfused systems [39, 40]. Particle Image Velocimetry (PIV) is an optical technique that allows the visualisation of flow inside transparent structures. It allows measurement of the flow's instant local velocity field by recording the movements of tracer particles that move with the fluid [41]. The basic set up consists of a high-speed camera which records the movements of the tracers illuminated by a pulsating light source. The videos are post-processed with algorithms that calculate the local velocity fields from the particle displacements and the frame rate. Micro Particle Image Velocimetry (μPIV) has previously been used to measure instantaneous and ensemble-averaged flow fields in micron-scale fluidic devices [42] using 100-300 nm diameter tracer particles. However, the μPIV technique has not been used to characterise flow inside porous cell scaffolds for perfused applications. Since one of the main problems with the current BALs is a poor mass transfer between hepatocytes and blood [11], the flow characterisation with μPIV and the bioreactor design optimisation to enhance mass exchange could improve device performance over time.

The purpose of this study was to develop a super-macroporous, biocompatible, non-biofouling BAL prototype, using PIV to characterise flow and inform an optimised bioreactor design to support high functioning hepatocytes. It was hypothesised that HEMA-based cryogels functionalised with alginate and RGD peptide could help to prevent non-specific protein adhesion and enhance cell adhesion. It is important to prevent protein adsorption from surrounding biological fluids to avoid pores occlusion and blood adhesion and inflammation. HEMA was chosen as scaffold material because it is a well know biocompatible, inert and low cost polymer commonly used in biomedical devices [13]. Alginate is a natural polymer containing negative charges which create a thick layer of water molecules and prevents proteins and cell adhesion from surrounding liquids, creating a non-fouling surface [43], whilst the RGD sequence binds to the membrane protein integrin receptor of most cell types [44, 45]. The internal flow inside cryogels was characterised using μPIV to quantify the flow velocity and vorticity. Flow characterisation inspired the development of a multi-layered bioreactor design in which cryogel discs seeded with hepatocytes are spaced to enhance the mixing of nutrients and oxygen before entering the next layer. This system would improve the mass exchange between hepatocytes and blood inside the cryogel pores, otherwise not promoted by the laminar nature of the flow. This new PIV-inspired cryogel-based multi-layered device was compared with the column version in terms of hepatocyte viability and functionality to potentially improve cryogel based bioartificial liver design

parameters. The optimised cell-free device was then assessed for safety using an *in-vivo* bile-duct ligation (BDL) disease rat model of liver cirrhosis.

2. Materials and methods

2.1. Materials

2-hydroxyethyl methacrylate (HEMA), polyethylene, poly(ethylene glycol) diacrylate (PEGDA, Mn 250), N,N'-methylenebis(acrylamide) (MBA), sodium alginate, *N,N,N',N'*-tetramethylethylenediamine (TEMED), ammonium persulfate (APS), triisopropylsilane, glass wool, sodium chloride (NaCl), cyanogen bromide (CNBr), bovine serum albumin (BSA), fluorescein isothiocyanate (FITC), MTT powder were purchased from Sigma Aldrich. (2-(1*H*-benzotriazol-1-yl)-1,1,3,3-tetramethyluronium hexafluorophosphate, hexafluorophosphate benzotriazole tetramethyl uronium) (HBTU), N,N-diisopropyilethylamine (DIPEA), piperidine, were purchased from AGTC. Fmoc rink amide linker and Tentagel S-NH$_2$ resin were purchased form Iris biotech GMBH. N,N-Dimethylformamide (DMF) was obtained from Fisher Chemical. Diethyleter (HPLC grade), methanol (HPLC grade), dichloromethane, sodium dodecyl sulphate (SDS) were obtained from Fisher Scientific. Fmoc amino-acids were purchased from Novabiochem. 40 % acrylamide/bis solution 19:1, mercaptoethanol and laemli buffer were obtained from Bio-Rad. LIVE/DEAD^{TM} Cell Imaging Kit, Dulbecco's modified eagle medium (DMEM), minimum essential media (MEM), Non-Essential Amino Acids Solution (100X), Trypsin-EDTA (0.25%), phenol red, Dulbecco's phosphate-buffered saline (DPBS), Penicillin-Streptomycin (10,000 U/mL) were obtained from ThermoFisher. Serum Albumin Human SimpleStep ELISA Kit was obtained from Abcam.

2.2. Synthesis of cryogels

HEMA-containing cryogels were synthesised by cryogelation technique (Fig. 1 A). Two different cross-linkers, PEGDA and MBA, were used to cross-link HEMA. Briefly, a monomer solution consisting of 0.891 ml of HEMA and 0.237 ml of PEDGA or 0.266 g of MBA in 20 ml DI water was degassed for 10minutes. 20 µl of TEMED was added, and the solution was cooled in ice for 15 minutes. 20 mg of APS was added and the solution was poured into 9 mm diameter glass tubes and incubated for 18 hours in a cryobath at -12 °C. After thawing, the cryogels were rinsed in deionised water and stored at 4 °C. Alginate was incorporate with two strategies. In the first, a solution of 1% (wt/vol) of alginate in deionized water was prepared. HEMA and cross-linker were added and the solution was degassed for 10 minutes with a vacuum pump. 20 µl of TEMED was added, and the solution was cooled down in ice. 100 µl of 50% glutaraldehyde solution was added with the APS. Cryogels were prepared at -12 °C as described above. In the second strategy, alginate was incorporated by post-synthesis surface modification. After synthesis, cryogels were immersed in a 0.03 M glutaraldehyde solution in acidic

conditions, obtained by adding 300 µl of a 1M HCl solution, and left for 2 hours on an orbital shaker for activation. Cryogels were then washed and put in a 1% (wt/vol) alginate solution overnight on an orbital shaker at a speed of 100rpm, washed and stored at 4 °C in DI water. Alginate-containing cryogel were incubated overnight in a 0.5 M glycine solution in phosphate buffer to block non-reacted aldehyde groups.

2.3. Synthesis of RGD-containing peptide

RGD-containing peptide was synthesised using a solid-phase peptide synthesis method, described by Merrifield et al. [46, 47], with the sequence GGWGGRGD. A tryptophan residue was added to the peptide tail to make it detectable by spectrophotometry. Prior to use, peptide was cleaved from the resin using a cleavage solution composed of TFA, triisopropylsilane and DI water and then purified by washing with diethyl ether. For Time-of-Flight mass spectroscopy (ToF-MS) and high-performance liquid chromatography (HPLC) characterisation, 1 mg of peptide was placed in a dried glass vial and dissolved in 1 ml of methanol.

2.4. Functionalisation of cryogel surface with RGD-containing peptide

Cryogels were functionalised with RGD peptide activating the hydroxyl groups with cyanogen bromide (CNBr) [27]. Cryogel columns were placed in tubes and connected through 2-stop silicon tubes to a multichannel peristaltic pump. The flow rate was set at 2 ml/min. Cryogels were washed with DI water, NaCl solution and sodium carbonate buffer, consecutively. A solution of 0.5 M of CNBr in sodium carbonate buffer was recirculated for 1 hour. Cryogels were then washed with sodium carbonate buffer. 30 mg of RGD-peptide were then dissolved in 40 ml sodium carbonate buffer and recirculated for 2 hours. Cryogels were then washed with a 1.0 M solution of ethanolamine (pH 9), NaCl solution and DI water. The RGD solution was collected before and after the functionalisation of each cryogel and analysed with a NanoDrop Lite spectrophotometer to check peptide loading.

2.5. Physicochemical characterisation

2.5.1. FTIR characterisation

Cryogel samples were freeze-dried and ground to a fine powder, and spectra were obtained in the range of 400-2000 cm^{-1} by 64 scans with 2 cm^{-1} resolution using Fourier-transform infrared spectroscopy (FTIR) performed with a Universal ATI, PerkinElmer (Spectrum 650) FT-IR spectrometer.

2.5.2. Zeta potential measurements

Cryogels were cut into small portions and freeze-dried overnight. The dried cryogels were then finely ground and suspended in DI water at a concentration of 0.25 mg/ml. A folded capillary cell (DTS1070) was filled with the cryogel solutions and zeta potential was recorded using Malvern Zetasizer Nano ZS90.

2.5.3. Scanning electron microscope (SEM)

Samples were prepared by sectioning into 3 mm discs, freeze drying, mounting on a sample holder and sputter coating with a 4 nm thick layer of platinum using a Quorum (Q150TES) coater. SEM was carried out using a Zeiss Sigma field emission gun SEM (Zeiss NTS) at an accelerating voltage of 5 kV at 200× magnification.

2.5.4. Confocal imaging

Cryogel discs were stained with 50 μM Rhodamine B solution in PBS for 30 minutes. Discs were then repeatedly washed with PBS and analysed with a HeNe laser at an excitation/emission wavelength of 526/573 nm using confocal microscopy (Leica TCS SP5, Wetzlar, Germany).

2.5.5. X-ray micro-computed tomography

Cryogel samples were incubated with a 0.5 M $FeCl_3$ solution overnight and washed with DI water prior to freeze drying. Samples were then scanned with X-ray micro-computed tomography (μCT) to obtain a 3D reconstruction of the pore networks, overall porosity and the percentage of connected pores. The μCT system is based on an open type X-ray source 160 kVp at 200 μA, a high-precision air-bearing rotating stage and amorphous silicon (a-Si) sensor array detector acquiring 16-bit grey level with a pixel matrix of 4096 × 4096 at 100 μm [48]. The cryogel samples were scanned with 60 kV at 25 μA and an emission focal spot of approximately 1.5 μm. The integration time was set to use the full detector's dynamic range, at 2500 ms. The angle step between radiographies depends on the specific magnification and size of the projected object. Those values were chosen according to the Nyquist theorem and are equal to 0.075°. For determining the effective μCT resolution (2.769 μm) a calibration was performed using certified ruby spheres (Renishaw®, A-5000-7812: ball grade 5 according to ISO 3290, deviation of spherical form from the nominal shape of 0.13 μm) [49]. The quantitative analysis of geometry features requires segmentation. Image enhancement techniques were applied leading to a clear bimodal voxel intensity histogram and allowing the distinction in voids and solid material. From the generated 3D binary void matrix, the sample porosity was extracted. The overall porosity was estimated by simply counting the number of voxels assigned to the void space. For the effective porosity a connectivity analysis was performed, identifying the three-dimensionally connected pores, spanning the sample from one end to the other in the flow direction. The effective and absolute porosity were extrapolated for a representative cylindrical volume of the cryogel sample (diameter of 4.43 mm and height of 2.77 mm).

2.5.6. Mechanical testing

8 mm-thick cryogel discs were compressed orthogonally to the circular face through full thickness at a rate of 0.05 mm/s and the elastic modulus was obtained from the linear region of the stress-strain

curve (<25% strain) a TA.XTplus Texture Analyser. The moduli values were reported as the mean +/- SEM of 5 samples.

2.5.7. Flow rate measurements

Cryogel samples of 2 cm height were placed below a 1 metre high water column containing degassed DI water. Water was allowed to flow through the cryogel sample under gravity. The time for 1 ml to pass through was recorded and a flow rate was calculated [50].

2.5.8. Particle Image Velocimetry setup for fluid dynamics measurements

The µPIV setup was composed of a digital camera with a long-distance microscope objective, a purpose-built LED light source, a syringe or peristaltic pump and a purpose-built optical chamber that hosts the cryogel column (Fig. 4). Amorphous silicon dioxide (SiO_2) beads were chosen as tracers with diameters 9-13 µm, which are representative of blood cells (6-9 µm). The suitability of the SiO_2 particles for PIV measurements was confirmed based on their terminal velocity and the Stokes number. The terminal velocity was calculated as:

$$V_T = \frac{(\rho_p/\rho_w - 1)\, g\, d_p{}^2}{18\, \mu_w}$$

with where ρ_p is the density of the glass particles (2196 kg/m³), ρ_w is the density of the water at 20°C (998 kg/m³), d_p is the largest SiO_2 particle diameter (13 µm) and μ_w is the water's dynamic viscosity (9.31 x 10^{-4} m²/s).

The Stokes number is a dimensionless parameter which describes the behaviour of particles suspended in a flow. It represents the ratio of characteristic times for a solid particle and the flow in which it is immersed. In PIV applications the Stokes number is used as an indicator for the suitability of a particle to be used as a tracer, and calculated as:

$$Stk = \frac{t_0\, u_0}{l_0}$$

where t_0 is the relaxation time of the particle, u_0 is the velocity of the flow away from the obstacle and l_0 is a characteristic dimension of the obstacle, in general its diameter. If the Stokes number is much less than 1 then the particles follow the flow's streamlines accurately.

The Reynolds number is a dimensionless number which describes the nature of flow. It is defined by the ratio of inertial to viscous forces of the fluid. Low Reynolds numbers indicate a laminar flow regime, whereas flows with a high Reynolds number are dominated by inertial forces that lead to turbulence. The Reynolds number is calculated as:

$$Re = \frac{\rho \, u \, L}{\mu}$$

where ρ is the fluid density, u is the velocity of the fluid, L is a characteristic linear dimension and μ is the dynamic viscosity of the fluid.

If the Reynolds number is smaller than 1, then the relaxation time (t_0) can be calculated as:

$$t_0 = \frac{\rho_{\mathrm{p}} \, d_{\mathrm{p}}^2}{18 \, \mu_{\mathrm{w}}}$$

For the µPIV measurements the flow rate was fixed at 3 ml/min, the medium recirculated was deionised water, the tracer particle number density was 3920 particles/mm^3, the image acquisition frame rate was 30 Hz, and the number of frames recorded per video was 300. Frames were then analysed using PIVLab [51] in MATLAB to compute the displacement of the glass tracer particles. The local flow velocity and vorticity fields were then interpolated (Fig. 4 A-E). Visualising flow inside cryogels is particularly difficult due to the partial opacity of the porous structure. In order to address this issue, a face of the cryogel was sectioned to provide a flat plane which could be scanned by the µPIV setup. As expected, the microscope could not form images of the structures deep within the cryogel, but it was possible to image the subsurface pores and surrounding flow.

2.6. Biological characterisation

2.6.1. BSA adsorption by alginate modified and non-modified cryogel variants

Cryogels were cut into 5 mm thick discs and immersed in a 1 mg/ml BSA solution in DI water for 24 hours at 37 °C. Discs not immersed in the BSA solution were used as negative controls. Samples were washed 3 times with sodium phosphate buffer and 20 µl of FITC was added to each well and incubated for 2 days. Cryogel discs were then thoroughly washed with water and analysed using confocal microscopy with an excitation and emission wavelength of 495/519 nm.

2.6.2. Plasma protein adsorption by alginate modified and non-modified cryogel variants

Cryogels were cut into 2 mm thick discs and immersed in human serum plasma. Discs were incubated at 37 °C for 30 minutes, washed with PBS and 200 µl of laemmli buffer (1X) was added for 1 hour. The extracts and plasma control (1:20 dilution) were collected and denatured by addition of 5% 2-mercaptoethanol and5 minutes incubation at 95 °C. Samples were loaded on a polyacrylamide gel and run at 100 mV for 2 hours followed by Coomassie blue staining for 30 minutes and destaining with a solution of water, methanol and acetic acid in a ratio of 50/40/10. Images of the gel were then taken with a densitometer (Alpha Innotech MultiImage Light Cabinet Filter Positions). Total protein content

of the extract was quantified using the bicinchoninic acid (BCA) assay following manufacturer's instructions (Sigma-Aldrich).

2.6.3. Cell culture methods

Human healthy liver hepatocytes-7 (HHL7) were cultured in high glucose Dulbecco's modified Eagles' medium (DMEM) with 10% fetal bovine serum (FBS), 1% non-essential amino acid (NEAA) and 1% antibiotic (P/S). HepG2 (human liver hepatocellular carcinoma, ECACC 85011430) were cultured in minimum essential media (MEM) with 10% FBS and 1% NEAA. 3T3s (mouse swiss albino embryo fibroblast, ECACC 85022108) were cultured in high glucose DMEM with 10% FBS. The pH was maintained at 7.4, in a 37 °C humidified incubator with 5% CO_2. Medium was changed every 2 days and cells were passaged at 70% of confluency.

2.6.4. Immunocytochemistry to confirm HHL phenotype

HHL7 and 3T3 (control) and HepG2 (control) were seeded in triplicate on sterile coverslips at a density of 8000 cells/cm^2. Cells, incubated for 72 hours and washed with PBS, were fixed with 4 % paraformaldehyde for 5 minutes followed by washing with PBS and 0.1 % Triton in PBS. Blocking buffer, composed of 1 % BSA (wt/vol) and 0.1 % Triton-X in PBS, was added and incubated overnight at 4 °C. A solution of 10 μg/ml of mouse anti-human cytokeratin 7 and 8 primary antibodies was added to the cells and incubated overnight at 4 °C. A 2 μg/ml anti-mouse IgG secondary antibody solution was added for 4 hours following by washing with PBS. Cells were then imaged using a confocal microscopy using an excitation/emission wavelength of 495/519 nm for Alexa Fluor 488 and an excitation/emission wavelength of 405/488 nm to detect DAPI stained nuclei.

2.6.5. MTT assay

Cryogels were cut into 2 mm thick discs and sterilised in a 70 % (v/v) ethanol solution for 15 minutes following by UV irradiation. 2.5 x 10^4 cells were seeded onto each cryogel disc and incubated up to 1 week. A 0.5 ml solution of 10% MTT (5mg/ml) in media was then added to each cryogel discs and controls and incubated for 4 hours. Media was replaced by 0.5 ml DMSO and 100 μl aliquots were transferred to a 96 well plate and absorbance was read at 570 nm. Viable cell number was extrapolated from the standard curve of increasing cell number against MTT absorbance.

2.6.6. Live/dead assay

Cryogel discs were prepared, sterilised and seeded with 2.5 x 10^4 cells. A 0.1 ml of live/dead working solution, composed of calcein-AM and ethidium-homodimer-1, was added and incubated for 15 minutes at room temperature. Cells were then imaged with the confocal microscope using an excitation/emission wavelength of 495/515 nm for calcein-AM and an excitation/emission wavelength of 517/635 nm for ethidium-homodimer-1. Esterases within living cells cleaved the calcein-AM ester

bond to produce a calcein positive green fluorescence. Dead cells were permeable to ethidium-homodimer-1 and fluoresced red.

2.6.7. Column and multi-layered bioreactor set up

Bioreactors were composed of glass tubes (9 mm diameter, 100 mm height) closed by purpose-built connectors 3D-printed with PLA polymer, in which cryogels were housed. Silicon tubes were connected to the chambers, recirculating medium from reservoirs with a multichannel peristaltic pump set at a flow rate of 1 ml/min (Fig. 7B). For the column bioreactors, cryogels of 20 mm height were placed in the glass tube, after sterilisation with ethanol and UV light. 5×10^6 cells for each column bioreactor were harvested and re-suspended in 25 ml in the medium reservoir and recirculated in the incubator at 37 °C and 5 % CO_2. The multi-layered bioreactors (Fig. 7A) were composed of 10 stacks of 2 mm-height cryogel discs separated by 2mm-height PLA 3D-printed spacers. Cryogel discs were previously seeded with 5×10^5 cells and incubated for 4 hours and then stacked inside the bioreactor chamber alternating one cryogel disc and one spacer. Aliquots of medium were collected for quantification of albumin production and after 72h medium was replaced by 1 mM NH_4Cl containing medium for stimulation of urea production. Cryogels were then extracted from the chamber and stained with live/dead and DAPI solution for cell imaging.

2.7. Treatment of BDL animals with multi-layered cryogel-containing bioreactor

Experiments were conducted in accordance with local ethical approval and subject to the UK Animal Scientific Procedures Act (1986, amended 2012). Under general anaesthesia (isoflurane, induction at 5 % in oxygen, maintenance at 1 % in room air), all rats underwent bile duct ligation (BDL) and section to induce biliary cirrhosis as described previously [52]. Animals were left recover for 24 hours under close observation and then transferred to normal housing for 4 weeks. The day of the experiment, animals were anaesthetised with isoflurane (induction at 5 % in oxygen, maintenance at 1 % in air for the length of the experiment) and catheters were inserted in the left carotid artery and in the right jugular vein. Blood was drawn via the arterial catheter using a peristaltic pump and returned through the jugular vein. The total circuit volume was less than 3ml, with the animals receiving a corresponding amount of normal saline to compensate for circuit volume and prevent hypovolaemia. Flow rate was set at 3 ml/min for all the duration of the experiment which was 3 hours in total. The control animal was not connected to the device but had corresponding surgery and had catheters placed for monitoring and blood sampling. Mean arterial pressure (Biopac US) and core temperature body were recorded every hour. Blood samples were taken every hour and placed into ice-cold lithium heparin coated tubes and centrifuged to separate plasma (3000 rpm, 4°C, 10 mins), which was stored at -80°C for subsequent biochemical analysis (Fujifilm Medical, UK – albumin, creatinine, bilirubin, urea,

glucose, AST). At the end of the experiment, blood and tissue were collected under terminal anaesthesia for future analysis.

2.8.1. SEM images on cryogel discs post BDL experiment

Cryogel discs that composed the multi-layered devices were removed from the bioreactor chamber, washed with heparinised saline solution and fixed in 4% formaldehyde for 1 hour and stored in ethanol at 4 °C. Samples were then washed three times with 2 ml of 0.1 M cacodylate buffer and frozen at − 80 °C and freeze-dried overnight. The freeze-dried cryogel discs were mounted on a sample holder and coated with a 4 nm thick layer of platinum with a Quorum Q150TES (Quorum) coater. Samples were then imaged using a Zeiss Sigma field emission gun SEM (Zeiss NTS) at an acceleration voltage of 5 kV.

2.8. Statistical analysis

Data are presented as mean ± standard deviation for at least three replicates. Statistical analysis was performed using a t-test or one and two way ANOVA with Bonferroni post-test, applying the correction for multiple comparisons at a significance level of $p < 0.05$ with Graph-Pad Prism 5 for Windows (GraphPad Software, USA).

3. Results

3.1. HEMA-based cryogel physicochemical characterisation

Two different cross-linkers, PEGDA and MBA, and two different strategies for alginate incorporation, pre and post synthesis, were first investigated to find the optimal formulation to produce suitable HEMA-based cryogels for this application in terms of physical and mechanical properties. All synthesised cryogel formulations possessed a continuous, opaque, sponge-like elastic structure (Fig. 1B) and retained shape memory. The internal microstructure consisted of an interconnected network of large, channel-like and open pores up to 100 μm, visible from SEM and confocal images (Fig. 2), which easily allowed liquids to pass through. In particular, HEMA-based cryogels cross-linked with PEGDA possessed a more regular distribution of pores than the cryogels cross-linked with MBA. μCT 3D reconstruction gave similar observations of the internal structure (Fig. 1C) where it is possible to see the pore walls (blue) and the void spaces between them (grey). The overall porosity of the HEMA-MBA cryogel was found to be 88.76 % from μCT scans, while the percentage of connected pores was 88.75 %.
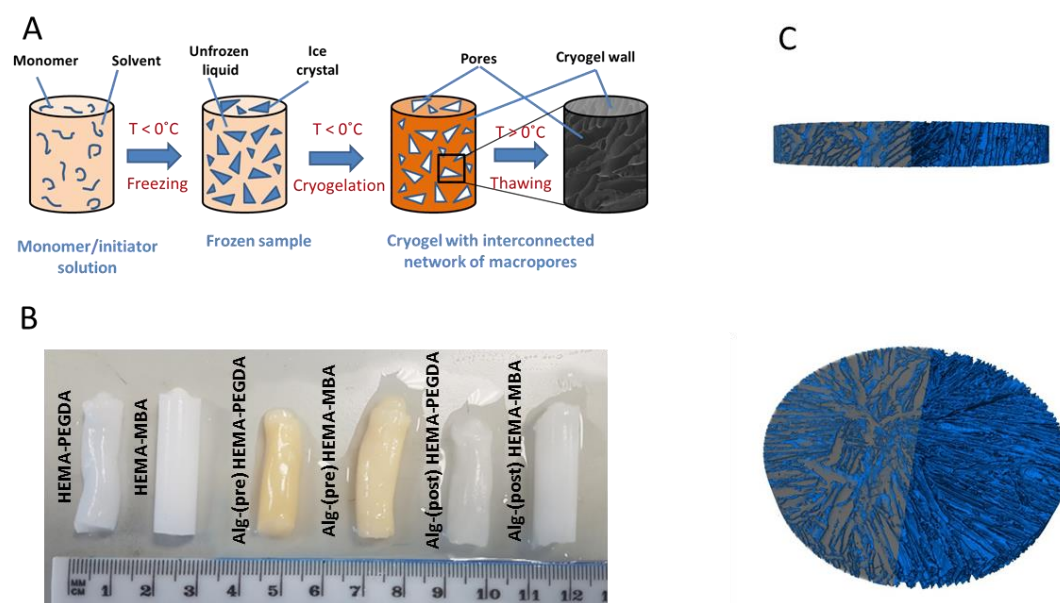
Fig. 1. A) Different stages of the cryogelation process. B) Photograph of synthesised cryogels. C) 3D X-ray µCT reconstruction of a HEMA-MBA cryogel sample, with the cryogel rendered in blue and pores filled in grey in the left half of the scan.
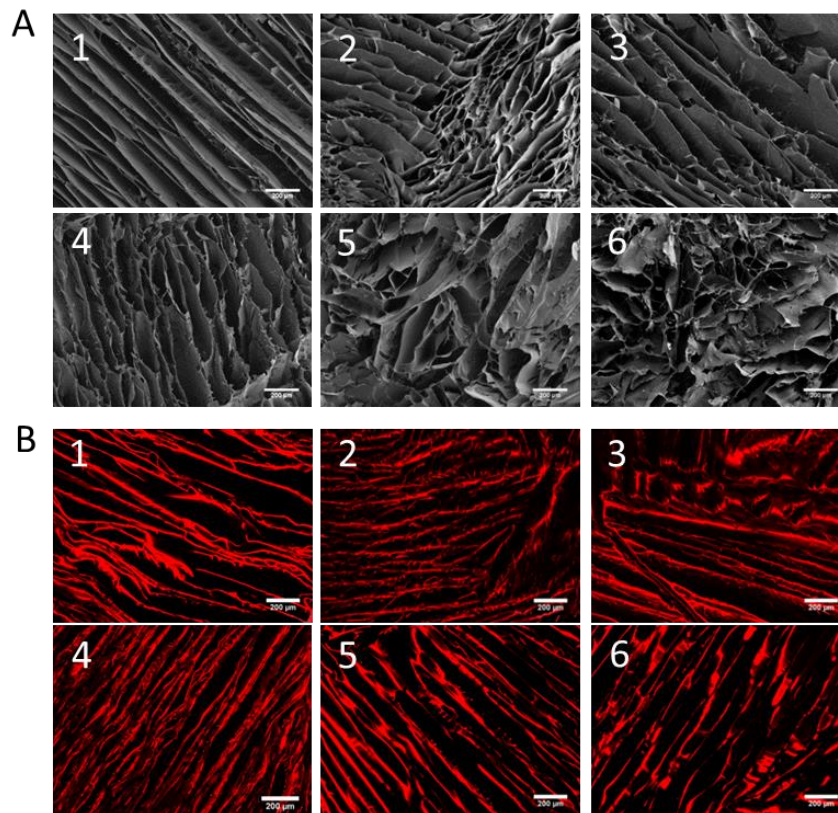

Fig. 2. Representative SEM (A) and confocal (B) images of synthesised cryogels. 1) HEMA-PEGDA, 2) Alg-(pre) HEMA-PEGDA, 3) Alg-(post) HEMA-PEGDA, 4) HEMA-MBA, 5) Alg-(pre) HEMA-MBA, 6) Alg-(post) HEMA-MBA. Scale bar 200µm.

Two different alginate incorporation strategies were investigated; in the first, alginate solution was mixed with monomer and cross-linker before cryogelation, whilst in the second, alginate was added to the cryogel surface post synthesis. From the FTIR spectra (Fig. 3A) it was possible to see the typical –COO$^-$ band of the alginate at 1600 cm^{-1} [53], confirming its incorporation in both of the alginate versions. Alginate also affected the total charge of the cryogels, measured by zeta potential analysis, (Fig. 3B). HEMA cryogels possessed a negative charge of -23 $\pm$ 0.9 mV for HEMA-PEGDA and of - 18.3 $\pm$ 0.4 mV for HEMA-MBA derived from the presence of the hydroxyl groups which are polar and at moderate to high pH function as an acid [55]. Alginate introduced a more negative charge to the PEGDA-cross-linked cryogels of $-$ 36.6 $\pm$ 1.1 mV and $-$ 34. 6 $\pm$ 0.9 mV in case of alg-(pre) and alg-(post), respectively, and for MBA-cross-linked cryogels it was $-$ 36.7 $\pm$ 1.1 mV and to -33.9 $\pm$ 1.0 mV in case of copolymerisation (pre) and functionalisation (post), respectively. The two methods of alginate incorporation gave similar results for both cross-linker types.

Regarding the mechanical properties, cryogels synthesised with MBA showed a significantly higher compressive modulus compared to those cross-linked with PEGDA of approximately 3 times higher, which were in the range of 11.2-12.6 kPa and 3.2 – 4.3 kPa for cryogel crosslinked with MBA and PEGDA, respectively (Fig. 3C). Amongst the cryogels with the same cross-linker, it was found that alginate incorporation, both by copolymerisation and functionalisation, did not significantly alter the mechanical properties of the resultant cryogels. The compressive modulus values for non-modified HEMA-PEGDA were 3.2 $\pm$ 0.9 kPa and for alginate-modified 4.3 $\pm$ 1 kPa and 3.0 $\pm$ 1.2 kPa for alg-(pre) and alg-(post) HEMA-PEGDA respectively. Similar for HEMA-MBA cryogels, compressive modulus was 11.2 $\pm$ 2.5 kPa, 12.0 $\pm$ 5.1 and 12.6 $\pm$ 2.6 kPa for non-modified, alg-(pre) and alg-(post) HEMA-MBA cryogels. Regarding the flow rate analysis, (Fig. 3D), HEMA-PEGDA cryogels, both with alginate and without, showed a heterogeneous behaviour to the water column. Some samples collapsed under the hydrostatic pressure, making impossible the measuring of the flow rate. HEMA- MBA cryogels showed a greater consistent behaviour to the water column and all the samples were able to sustain the hydrostatic pressure, allowing the water to pass through. Regarding the alg-(pre) HEMA-MBA cryogels, the recorded flow rate was significantly lower, of 2.3 $\pm$ 0.47 ml/min, compared to plain cryogel, which had 8.4 $\pm$ 3.5 ml/min. Regarding the cryogel modified with alg-(post) the flow rate was of 3.7 $\pm$ 0.1 ml/min, which was lower than plain cryogels but not significantly different.

Fluid dynamic measurements were conducted only on plain HEMA-MBA cryogels since the internal structure and pore size were very similar to the alginate modified (post) version (Fig. 2) and also the flow rate was not significantly different (Fig. 3D). Local Reynold numbers were calculated for 7 flow videos obtained with both syringe and peristaltic pumps. This was conducted to investigate whether

the motion created by different pump types affected the flow. The Reynolds numbers were 0.076 ± 0.007 and 0.233 ± 0.122 for videos taken with syringe and peristaltic pump, respectively. For both types of pumping systems, the Reynolds number was confirmed to be less than 1, confirming that the SiO_2 particles followed the flow accurately. The terminal velocity was calculated as 0.119 µm/s, which is significantly smaller than the typical flow velocity (20 µm/s), confirming that the particles will settle in a quiescent body of fluid. The Stokes numbers of the glass beads moving with the fluid was then calculated and found to be substantially less than 1 for both types of pump. Both the syringe and peristaltic pumps gave similar local velocities, which are in the order of 10^{-5} m/s. The cyclic motion introduced by the peristaltic pump resulted in oscillations of the flow, but the PIV analysis demonstrated that this did not introduce significant vorticity or transient turbulent flow patterns (Fig. 4) for the range of flow rates normally used for cell-perfused devices (up to 10 ml/min).
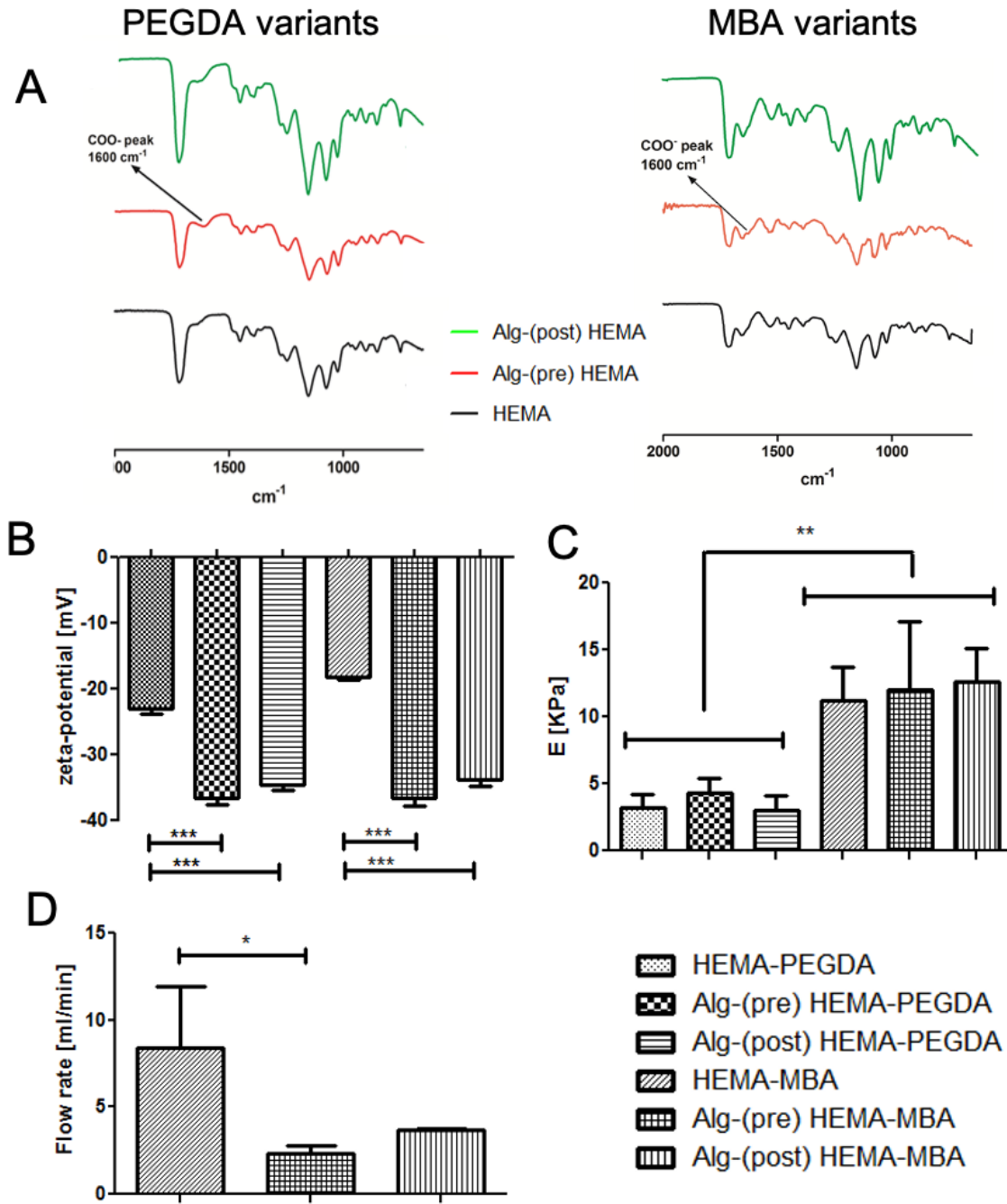
Fig. 3. A) FTIR spectrum of alginate and plain cryogels. B) Z-potential measurements (n=9). C) Elastic modulus obtained by unconfined uniaxial compression of the cryogels (n=5). (D) Flow rate across the cryogel columns (n=3). Values represent mean ± SD. Statistical analysis performed using ANOVA with Bonferroni's post-hoc test (***p < 0.001, **p < 0.01, *p < 0.05).
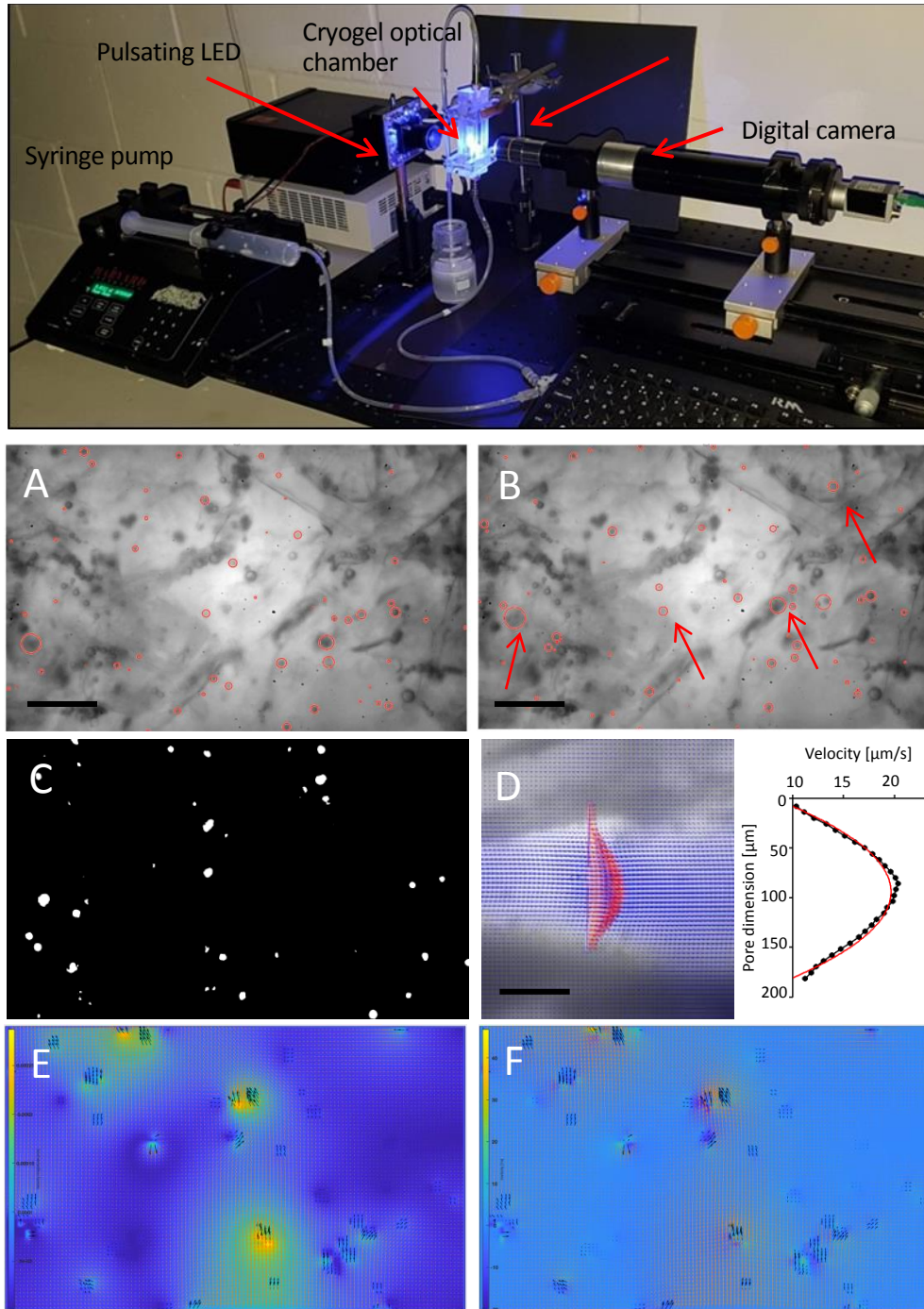
Fig. 4. Top: μPIV set up used to record flow inside cryogels using glass beads as tracers. Bottom: Process to extrapolate velocity profiles, local velocities and local vorticities from videos recorded with the high-resolution microscope inside the cryogel matrix. Videos were processed in MATLAB to obtain the frames, each separated by fixed frame rate. A and B show two consecutive frames of the same video in which particles can be seen to move along the channels. Scale bar 100 μm. Image processing was applied to detect the glass beads (C), and the flow field was obtained using a PIV algorithm to calculate the particle displacement vectors from frame to frame. Another MATLAB script was implemented to obtain the average velocity profile in customized positions in the map (D). In this example, the velocity profile was calculated perpendicularly to a longitudinal cryogel pore. Scale bar 100 μm. The maximum velocity was obtained at the centre of the pore and was of 20 μm/s. Instantaneous local velocity (E) and instantaneous vorticity (F) maps for each frame of the video were then extrapolated with PIVlab tool.

3.2. BSA and protein adsorption studies by alginate modified and non-modified cryogel variants

Incorporation of alginate resulted in a reduction in the adsorption of proteins from BSA solution and human plasma by HEMA-MBA cryogels analysed using FITC fluorescent labelling, BCA assay and SDS-PAGE. In particular, from the confocal images of the BSA adsorption experiment (Fig. 5A 1-2) it was possible to see that the alginate-modified cryogel had a significantly reduced FITC fluorescent signal comparing to the control. The absorbance of the eluted plasma solutions after mixing with the BCA reagents was 0.664 ± 0.037 from the HEMA-MBA cryogel and 0.191 ± 0.066 from the alginate-(post) HEMA-MBA cryogel (p< 0.001) (Fig. 5B). This result was in agreement with the SDS-PAGE gel electrophoresis of the same samples (Fig. 5C) in which the protein bands of the samples extracted from the alginate cryogels were less intense than the plain controls, indicating less protein adhesion to the plain cryogel.
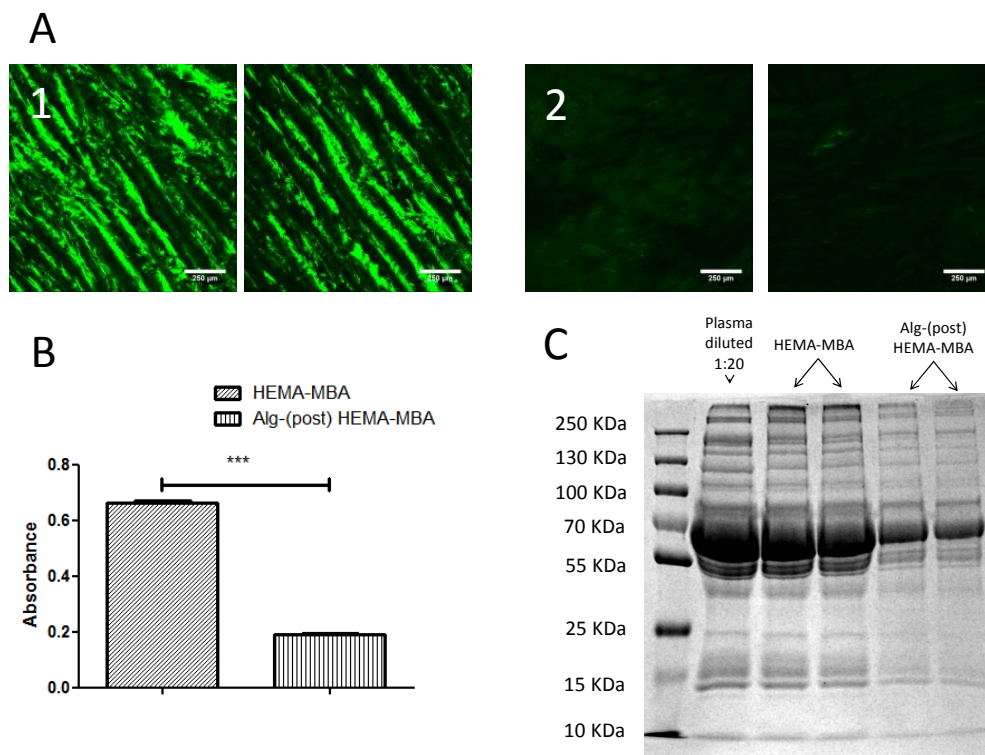

Fig. 5. Protein adsorption studies. A) Representative confocal images of HEMA-MBA cryogels (1) and alg-(post) HEMA-MBA cryogel (2) after immersion in the BSA solution and stained with FITC. BSA proteins bound to FITC gave a fluorescent signal when excited at 495 nm. Scale bar 250 μm. B) BCA total protein assay performed on the sample extracts taken from cryogels after immerging in human plasma solution. C) Gel electrophoretic bands of the molecular ladder, of 1:20 diluted plasma, of two HEMA-MBA replicates, of two alg-(post) HEMA-MBA replicates. Values represent mean ± SD. Statistical analysis performed using a t-test (*p < 0.001).**

3.3. Immunocytochemistry to confirm HHLs phenotype

The immunocytochemistry confocal images for the CK8 and CK7 parenchymal and non-parenchymal markers of HHL7, HepG2 and 3T3 are shown in Fig. 6A. Accordingly with Clayton et al. [54], HHL7 cells possessed both markers confirming maintenance of the HHL7 phenotype, whilst HepG2 only expressed the non-parenchymal marker CK8. The negative control 3T3 fibroblast cells did not express the two markers.

3.4. Static cell viability studies

Cell viability on RGD-alg-(post) cryogels and alg-(post) cryogels was analysed by MTT and live/dead confocal imaging. The quantification of living cells by MTT over time (Fig. 6B left) showed that cell viability was significantly higher on the RGD modified cryogels compared to the peptide free controls ($p < 0.001$). This result was supported by an increased calcein-positive cell fraction across the RGD modified cryogels, showed by the live/dead confocal images (Fig. 6B right). More fluorescent staining can be seen across the surface of the RGD modified cryogels indicating improved cell adhesion characteristics.
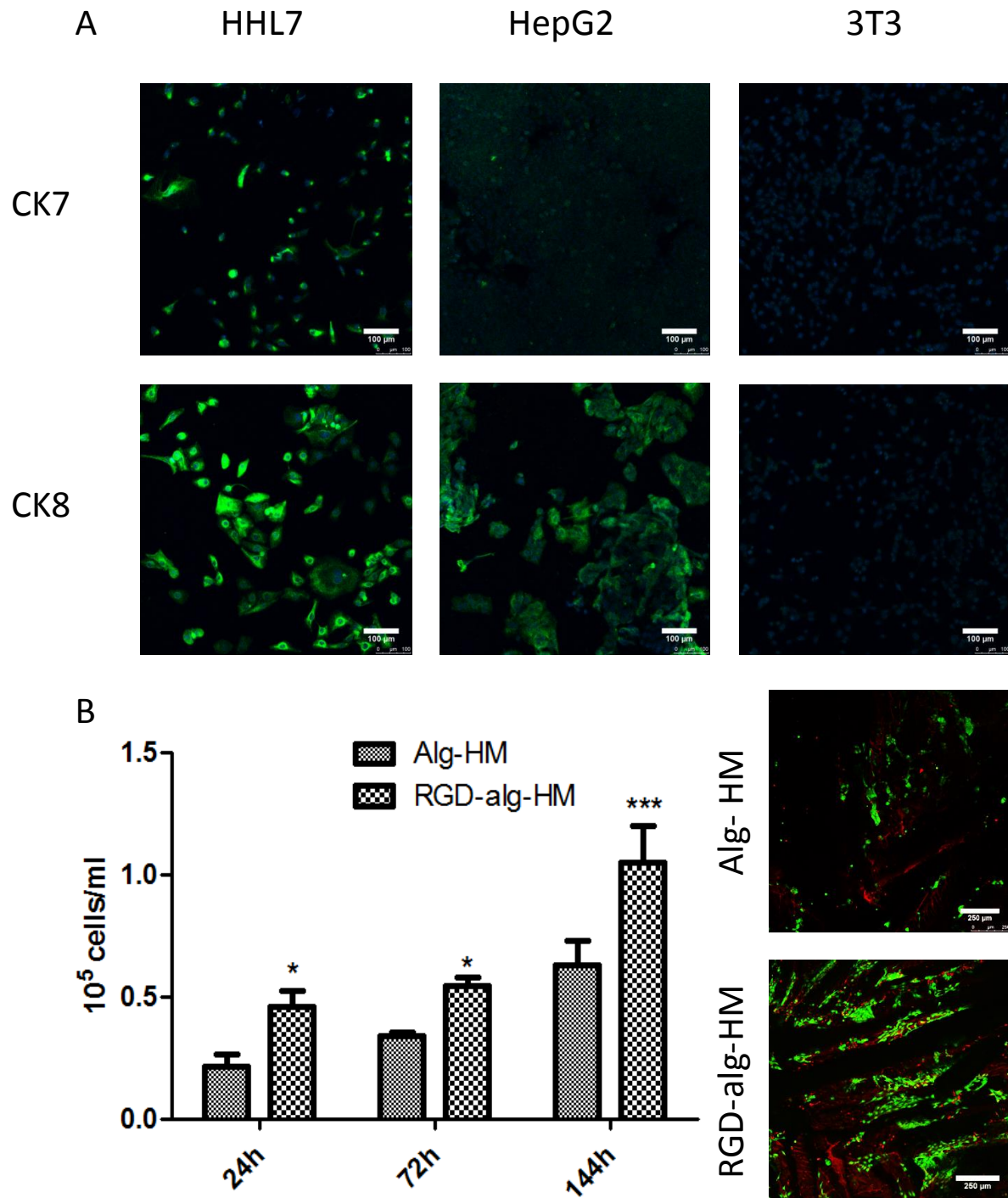
Fig. 6. A) Immunocytochemistry of parenchymal and non-parenchymal (CK7 and CK8) markers on HHL7, HepG2 and 3T3. Scale bar 100 μm. **B)** (left) Cell viability assayed by MTT on alginate-(post) cryogels containing RGD and without (n=3). (right) Representative live/dead confocal images of HHL7 cells seeded on alg-(post) HEMA-MBA (left) and RGD-alg-(post) HEMA-MBA after 120 h of culture. Green represents living cells; red represents dead cells. Scale bar 200 μm. Values represent mean ± SD. Statistical analysis performed using ANOVA with Bonferroni's post-hoc test (***$p < 0.001$).

3.5. Flow study to compare functional performance of column and multi-layered cryogel bioreactors

The two different types of bioreactors, column and multi-layered, were compared in terms of cell viability and the production of albumin and urea (Fig. 7B). From the confocal live/dead images, (Fig. 7C, D) hepatocytes were visible across the entire surface of the cryogel matrix in the multi-layered bioreactor whilst they were present only in the top layer of the column bioreactor. Cell viability was maintained throughout the length of the multi-layered bioreactor whilst cells were dead or not present inside the column device. Albumin production measured at 24h and 72h in the multi-layered bioreactor was respectively 1.02 ± 0.04 ng/ml and 3.48 ± 0.8 ng/ml and was significantly higher (p< 0.001) than the albumin produced in the column bioreactor, which was 0.00 ± 0.00 ng/ml at 24 h and 1.79 ± 0.03 ng/ml at 72 h. Urea production measured at 6 h and 24 h after stimulation with NH_4Cl in the multi-layered bioreactor was respectively 0.11 ± 0.02 mg /dl and 0.41 ± 0.01 mg /dl and was significantly higher (p< 0.001) than the urea produced by the column bioreactor, which was 0.09 ± 0.01 mg/dl after 6 h and 0.25 ± 0.02 mg/dl after 24 h. These results are showed in Fig. 7E.
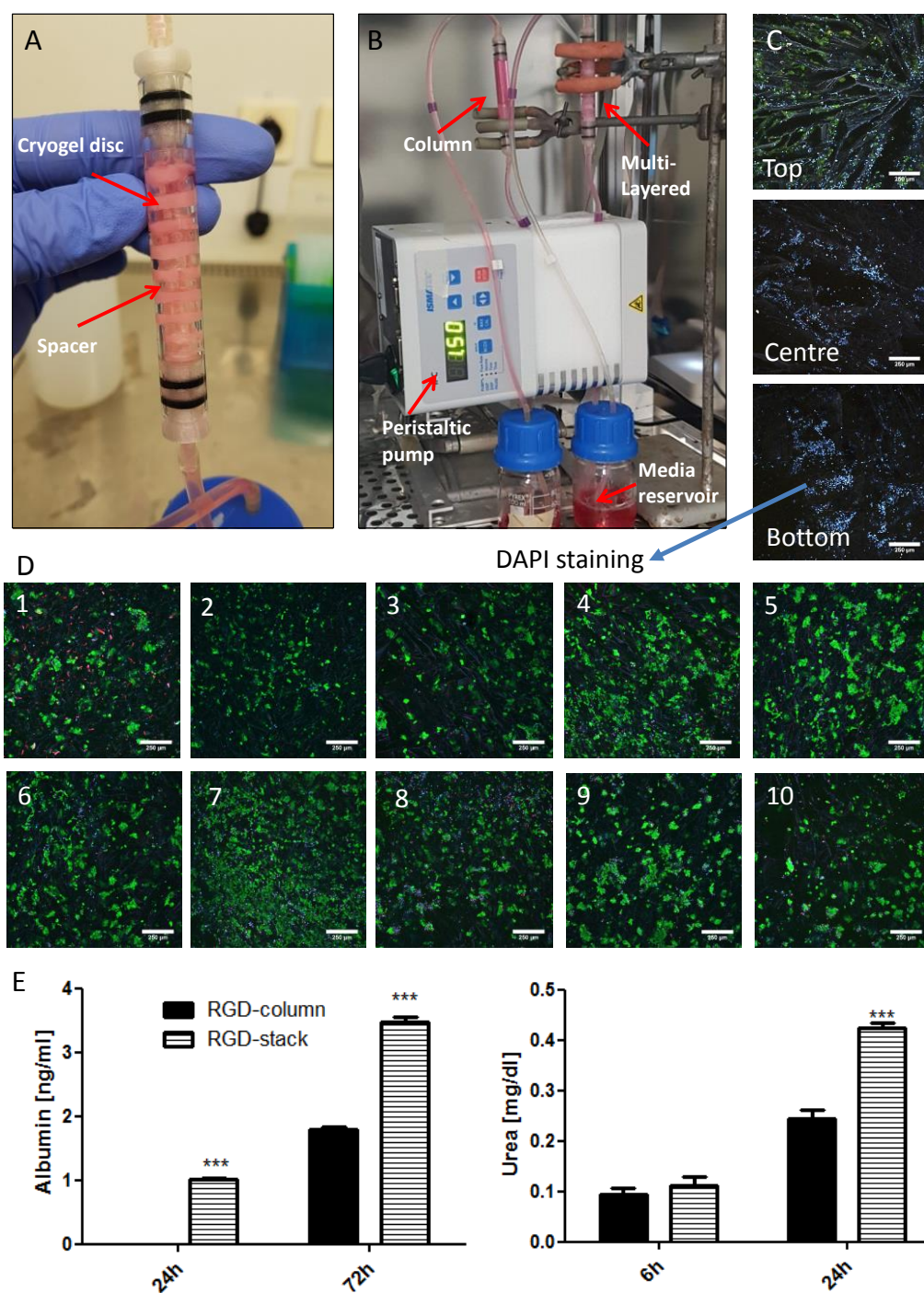
Fig. 7 A) Multi-layered bioreactor composed of ten cryogel discs and 3D printed spacers. B) Column and multi-layered bioreactor setup. C) Representative live/dead confocal images of the top, centre and bottom sections of the column bioreactor. DAPI staining highlighted with the arrow. D) Representative live/dead confocal images of the 10 cryogel discs that composed the multi-layered bioreactor. 1 is the top disc going down to 10 which is the bottom disc. Green represents living cells; red represents dead cells. E) Albumin production on column and multi layered bioreactors (n=3) at 24 h and 72 h and urea production after 6h and 24h post stimulation with ammonium chloride on column and multiplayers bioreactors (n=4). Values represent mean ± SD. Statistical analysis performed using ANOVA with Bonferroni's post-hoc test (***$p < 0.001$). Scale bar on all C and D images is 250 μm.

3.6.   Treatment of BDL animals with multi-layered cryogel-containing bioreactor

Treatment of the BDL rat with the cryogel device (Fig. 8 A) demonstrated safety and tolerability over the 3-hour period of the study. This duration is imposed by the limitation of the protocol for ensuring the well-being and monitoring of the animals. The BDL model was chosen as being representative of subjects with liver disease and their pathophysiology and thought a better test of the novel material design performance than would be observed using healthy control animals. This is because a BDL animal possesses compromised liver function which also affects the inflammatory response to a new material, as would happen in a patient with liver disease. There were no incidents of clotting or bleeding in any of the studies indicating good biocompatibility. Blood pressure was readily maintained and there were no fluctuations in temperature that would have indicated an inflammatory response (Fig. 8 B). The cryogels maintained their mechanical structure intact and their open porosity as shown by the SEM images taken after the experiment (Fig. 8 C). Blood biochemistry analysis on blood samples taken at the beginning and the end of the perfused experiment and controls indicated no adverse effects from cryogel perfusion and are reported in Table 1.
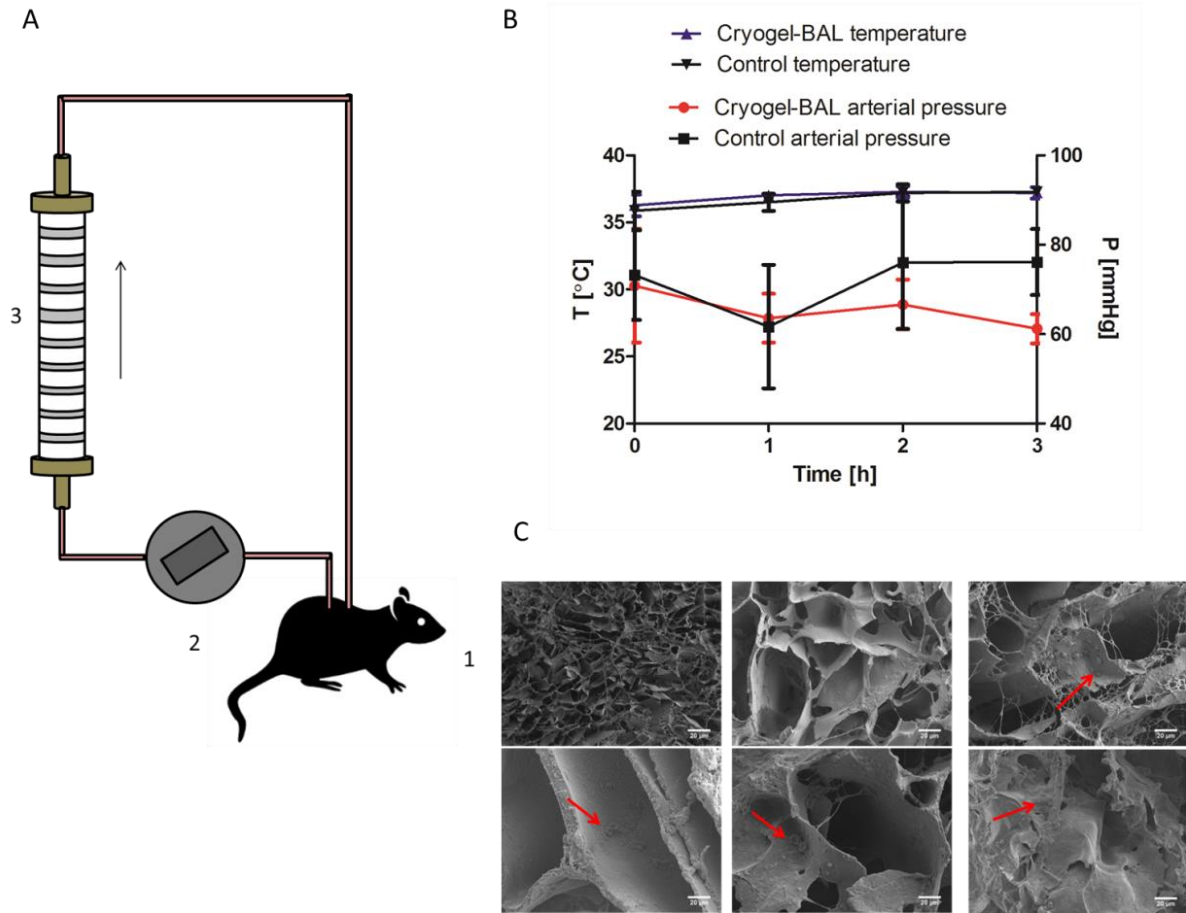
Fig. 8. Cell-free cryogel-BAL in vivo safety study in a BDL rat model of liver cirrhosis. A) BDL animal model experimental setup. 1- BDL rat, 2- peristaltic pump set at 3 ml/min, 3- cryogel containing bioreactor. B) Core temperature and blood pressure recorded during the BDL experiment (n=3). Values represent mean ± SD. C) SEM images of the cryogel discs that composed the bioreactor after BDL experiment. Arrows indicate red blood cells. Scale bar 20 μm.

Table 1. Blood biochemistry values analysed on blood samples taken from BDL rats treated with cell-free cryogel-BAL and controls. (mean ± SD, n =3).

		Cryogel-BAL		Control	
		T=0 h	T=3 h	T=0 h	T=3 h
Albumin	[g/L]	18.67 ± 3.30	16.67 ± 1.70	15.02 ± 8.70	19.16 ± 2.24
Creatinine [μmol/L]		19.67 ± 3.68	47.00 ± 17.28	24.37 ± 4.14	24.37 ± 4.14
Bilirubin [μmol/L]		129.00 ± 9.63	114.67 ± 15.92	406.90 ±131.7	280.60 ± 116.06
Urea [mmol/L]		4.71 ± 0.71	9.55 ± 1.53	3.6 ± 0.47	6.27 ± 0.88
Glucose [mmol/L]		7.13 ± 0.75	8.07 ± 1.30	5.24 ± 2.90	4.44 ± 0.23
ALT	[U/L]	54.00 ± 12.96	93.67 ± 25.10	80.27 ± 19.28	78.50 ± 15.00

4. Discussion

Whilst bioartificial liver bioreactors offer a potential route by which liver function may be replaced as a bridge to transplant or recovery, a design which adequately maintains liver function over time has yet to be achieved. This is because there is a need to simultaneously sustain a high metabolic hepatocyte fraction, to employ a bio and hemo compatible scaffold which prevent blood proteins and cell adhesion and enhance mass exchange between hepatocytes and blood. Cryogels offer a promising approach as a 3D scaffold to support a high fraction of metabolising hepatocytes and interconnecting macroporosity suitable for blood perfusion. In this study, a multi-layered bioreactor composed of discs of surface engineered HEMA-based cryogel with alginate and RGD was developed and tested for safety in a BDL animal model of liver disease.

HEMA-based cryogels were synthesised with different cross-linkers in order to select the most suitable formulation for this application, which include open porosity to support fluid permeation and pore size up to 100 μm to allow cell colonisation and proliferation [55]. Also adequate mechanical properties are required to sustain flow pressure without pore collapse. All the HEMA-based cryogels possessed open porosity, interconnectivity of pores and pore size up to 100 μm, which is in agreement with the previous study [27] and with current studies on cryogels [13, 26, 28]. The SEM and confocal images, Fig. 2, showed a similarity of the dehydrated and hydrated structure, respectively. This

indicates that the 3D structure is very stable and polymer walls do not swell much, maintaining interconnected porosity of cryogel in the swollen state. The pore interconnectivity is an important parameter since it indicates less resistance to flow and better accessibility of the scaffold surface for the cell population.

Cryogels synthesised with MBA were stronger and less compressible than the cryogels synthesised with PEGDA (p< 0.01), as showed in Fig 3 C, and able to sustain a 1 m column of water without collapsing with a measurable flow rate (Fig 3 D), whilst the cryogels synthesised with PEGDA collapsed under the pressure. The alteration of the mechanical properties might be due to the nature of the cross-linker as PEGDA is a longer and more flexible molecule (MW 400 g/mol) than MBA, (MW 154.17 g/mol), resulting in a more flexible structure. This difference in mechanical performance was maintained even after the introduction of alginate by both post- and pre-synthesis methods (Fig 3 C). For this reason, cryogels synthesised with PEGDA were discarded for further analysis.

It is interesting that the incorporation of alginate with both strategies did not significantly affect the compressive modulus of the resultant alginate-modified cryogels comparing to the plain version (Fig 3 C) whilst the flow rate diminished for the alginate-modified cryogel produced with the pre-synthesis method comparing to the plain version (Fig 3 D, p< 0.05). This reduction in the flow rate could be explained by blocking some small pores, which was not visible on the SEM and confocal images (Fig 2). The internal microstructure and pore size of the alginate-modified cryogels on SEM and confocal images appeared to be similar to the plain cryogel for both modification strategies. This underlines also that alginate modification did not obstruct the big pores, maintaining the resultant open porosity and interconnectivity of the cryogel microstructure. To ensure a sufficient flow rate, the post-synthesis modification strategy was then chosen to incorporate alginate onto HEMA-MBA cryogels.

Protein adsorption studies demonstrated that alginate modification helped to prevent protein adhesion from biological fluids. In particular, the BSA absorption study showed that alginate-post modified cryogels did not show a fluorescent signal after immersion in the BSA solution, whilst the plain version showed a strong fluorescent signal (Fig. 5A) indicating that alginate prevented the absorption of proteins. This result was confirmed also when cryogels were immersed in human serum plasma. From SDS-PAGE gel electrophoresis analysis (Fig. 5C) the bands of the protein extracts from the alginate modified cryogels were less dense than the plain cryogel. From the BCA assay performed on the same extracts, a similar result was achieved, Fig. 5C. Alginate reduced the absorption of plasma proteins by 70% (p< 0.001). The alginate-modified cryogels produced here showed improved non-fouling surface properties compared to cryogels used in previous studies for BAL applications [28].

The further surface functionalisation with the RGD peptide produced a cryogel with significantly enhanced cell adhesion and proliferation properties, as demonstrated by MTT and live/dead confocal images (Fig. 6B), which showed an increase of approximately 40% (p< 0.001) in cell density after 144 hours compared to the non RGD-containing cryogel.

A μPIV setup (Fig. 4) was used for the first time to visualise and characterise flow inside the porous cryogels. The flow measurements taken with the μPIV setup revealed that flow inside cryogels (at 3ml/min) was laminar with a Re < 1 and with little recirculation. The result obtained is in line with the qualitative approximation recently described for microflow in porous media [56] where flows with Re < 25 can be considered as Stokes flow.This suggested that the internal flow does not reorganise itself through the cryogel channels, even when a pulsating peristaltic pump is used. In this scenario, biological molecules and toxins in patient blood which stream at the centre of a channel cannot interact with hepatocytes seeded onto the pore walls. In order to enhance increase interaction between solutes and hepatocytes, a layered bioreactor (Fig. 7A) was designed to force a reorganisation of the flow at regular intervals. This multi-layered design was compared to the cryogel column version in terms of cell viability and functionality using a continuously circulating bioreactor setup. Cell viability was improved throughout the bioreactor length in the multi-layered design (Figs. 7C, D). Cells perfused through the column bioreactor were present in the column but were viable only on the top section (Fig. 7C), possibly due to a lack of oxygen and nutrients transport to the centre of the column, as suggested by the μPIV analysis. Results indicated that the column design and/or seeding method were not optimal for use in a flow perfused device, such as BAL, since most of the cryogel column were not colonised by cells, reducing efficiency. Flow reorganisation and seeding cells on cryogel discs prior to assembly as a multi-layered bioreactor allowed a viable and homogenous cell distribution throughout the device. Albumin and urea production were also significantly improved in the multi-layered design (Fig. 7E). Thus, the layered configuration allowed improved device performance compared to the column version.

Cryogel performance in the current study compares favourably to BAL cryogel prototypes previously examined in the literature in terms of reduced protein adsorption characteristics [28]. In the previous work, a single column cryogel made from an interpenetrating polymer network (IPN) of chitosan and poly(N-isopropylacrylamide) (poly(NiPAA) cryogel was used. HepG2 cells were incorporated at a seeding density 5 times higher ($2.5 * 10^7$ cells) than the HHL7 cell density used in the multi-stacked bioreactor assessed in this study. Whilst a direct comparison between the systems cannot be made since the cell source, culture conditions and set up parameters are different, the previous study

indicated a result of 90% plasma protein adsorption. In contrast, the current study indicated a significantly reduced plasma protein adsorption on surface modification of the HEMA-MBA cryogels with alginate as shown in Fig. 5B. Protein adsorption was reduced to less than 30% that of the plain HEMA-MBA cryogel indicating propensity for reduced biofouling on plasma perfusion. RGD peptide surface modification was then used to specifically increase cell adhesion as indicated by the viable cell adhesion study results shown in Fig. 6B. In addition, the current study indicated that use of a multi-stacked cryogel bioreactor rather than a single column bioreactor as in the previous study [28] is preferable. Metabolically active hepatocytes populated the entire bioreactor in the multi-stacked system (Fig. 7C) but only the upper section of the single column bioreactor (Fig. 7D).

A first pre-clinical study of the cell-free device was performed to assess safety using a BDL model (Fig. 8 A). Temperature and arterial pressure were stable during the length of the experiment and were not significantly different from the BDL controls (Fig. 8 B), indicating that no adverse inflammatory response resulted from cryogel perfusion within the experiment. SEM imaging following blood perfusion through the cryogels indicated no collapse of internal porous structure indicating suitability for use as a blood perfused device (Fig. 8 C). Furthermore, SEM imaging indicated minimal adhesion of red blood cells to the cryogel wall. It is anticipated that post-synthesis modification of the cryogels with alginate contributed to the suppression of protein adsorption to the cryogel walls and a subsequent reduction in blood cell activation and inflammation. Changes in blood biochemistry following perfusion through the cryogels were within the range expected from previous studies using the BDL disease model [57-59]. These results indicated that the cell-free cryogel-BAL device maintained similar vital parameters and blood biochemistry compared to BDL controls and to BDL models found in the literature, indicating safe use in an animal model of liver cirrhosis. Results were restricted to a cell free device in order to avoid activation of an immune response on blood contact with cells in the device and to establish markers of an inflammatory response initiated by the plain cryogel alone. Ultimately the device would be used within a plasmapheresis system to restrict bioreactor cell contact to plasma only. Here, a multi-layered cryogel-based BAL prototype suitable for being used in a small animal model was developed with encouraging preliminary results. A scaling up of the device will be performed to contain 10^9- 10^{10} cells for clinical studies. Cryogelation technology allows the production of cryogels of feasible size to contain and support this number of cells and to fit a bigger version of the device, whilst maintaining the same porosity and mechanical properties. Furthermore, since the device is made of layers of cryogel discs is also possible to create different units to be used in parallel or increasing the number of layers to support the right number of metabolising cells if necessary.

5. Conclusion

In this study a cryogel cell scaffold was designed for bioartificial liver with engineered surface properties and optimised fluid dynamics using for the first time a μPIV setup. The device inhibited non-specific protein biofouling and augmented viable hepatocyte metabolic function in a bioreactor test system. Post-synthesis alginate surface modification was protein inhibitory through increased negative surface charge with maintenance of mechanical and flow characteristics. RGD peptide incorporation significantly enhanced hepatocyte adhesion and metabolic activity. A μPIV setup was developed and used for the first time to visualise and measure the internal flow characteristics of a red blood cell simulant through the porous cryogel scaffolds. The results from PIV analysis were used to build a multi-layered scaffold bioreactor design in which introduction of flow reorganisation through cryogel disc stacking significantly improved hepatocyte adhesion throughout the bioreactor. The design reduced blood protein adhesion for repression of non-specific biofouling and altered column flow characteristics through a stacked design to significantly improve measures of bioreactor function. The results of the study suggest an improved cryogel bioreactor design for BAL compared to previously used single-column cryogel versions allowing better hepatocyte colonisation throughout the device. The use of the optimised cryogel-containing cell-free device in a BDL disease rat model of liver cirrhosis showed its safety in terms of vital parameters and blood biochemistry. The results obtained here indicate the feasibility of a multi-layered cryogel-cell scaffold as a new approach to BAL design informed by μPIV derived characterisation of internal flow. Furthermore, this study validated an optical method to analysis and improve fluid dynamics inside opaque and porous matrices which can be used to characterise other types of perfused systems where laminar flow could be an issue to diminish the device performance.

Data availability

The raw/processed data required to reproduce these findings cannot be shared at this time due to technical or time limitations

References

1. Blachier, M., et al., *The burden of liver disease in Europe: A review of available epidemiological data.* Journal of Hepatology, 2013. **58**(3): p. 593-608.
2. Kumar, A., A. Tripathi, and S. Jain, *Extracorporeal bioartificial liver for treating acute liver diseases.* The journal of extra-corporeal technology, 2011. **43**(4): p. 195-206.
3. Carpentier, B., A. Gautier, and C. Legallais, *Artificial and bioartificial liver devices: present and future.* Gut, 2009. **58**(12): p. 1690-1702.
4. Wang, Y., et al., *Current development of bioreactors for extracorporeal bioartificial liver (Review).* Biointerphases, 2010. **5**(3): p. FA116-FA131.
5. Ellis, A.J., et al., *Pilot-controlled trial of the extracorporeal liver assist device in acute liver failure.* Hepatology, 1996. **24**(6): p. 1446-1451.
6. Detry, O., et al., *Clinical use of a bioartificial liver in the treatment of acetaminophen-induced fulminant hepatic failure.* The American surgeon, 1999. **65**(10): p. 934.
7. Teotia, R.S., et al., *Bifunctional Polysulfone-Chitosan Composite Hollow Fiber Membrane for Bioartificial Liver.* Acs Biomaterials Science & Engineering, 2015. **1**(6): p. 372-381.
8. Palakkan, A.A., et al., *Evaluation of polypropylene hollow-fiber prototype bioreactor for bioartificial liver.* Tissue Engineering Part A, 2013. **19**(9-10): p. 1056-1066.
9. Coward, S.M., et al., *Alginate-encapsulated HepG2 cells in a fluidized bed bioreactor maintain function in human liver failure plasma.* Artificial organs, 2009. **33**(12): p. 1117-1126.
10. Chen, H.S., et al., *Randomized trial of spheroid reservoir bioartificial liver in porcine model of posthepatectomy liver failure.* Hepatology, 2019. **69**(1): p. 329-342.
11. Hou, Y.-T. and C.-C. Hsu, *Development of a 3D porous chitosan/gelatin liver scaffold for a bioartificial liver device.* Journal of Bioscience and Bioengineering, 2020.
12. Ding, Y.-T. and X.-L. Shi, *Bioartificial liver devices: Perspectives on the state of the art.* Frontiers of medicine, 2011. **5**(1): p. 15-19.
13. Savina, I.N., et al., *Cryogels from poly (2-hydroxyethyl methacrylate): macroporous, interconnected materials with potential as cell scaffolds.* Soft Matter, 2007. **3**(9): p. 1176-1184.
14. Gun'ko, V.M., I.N. Savina, and S.V. Mikhalovsky, *Cryogels: Morphological, structural and adsorption characterisation.* Advances in Colloid and Interface Science, 2013. **187**: p. 1-46.
15. Savina, I.N., et al., *A simple method for the production of large volume 3D macroporous hydrogels for advanced biotechnological, medical and environmental applications.* Scientific reports, 2016. **6**: p. 21154.
16. Vrana, N.E., P.A. Cahill, and G.B. McGuinness, *Endothelialization of PVA/gelatin cryogels for vascular tissue engineering: effect of disturbed shear stress conditions.* Journal of Biomedical Materials Research Part A, 2010. **94**(4): p. 1080-1090.
17. Plieva, F.M., I.Y. Galaev, and B. Mattiasson, *Macroporous gels prepared at subzero temperatures as novel materials for chromatography of particulate-containing fluids and cell culture applications.* Journal of Separation Science, 2007. **30**(11): p. 1657-1671.
18. Andaç, M., et al., *Molecularly imprinted composite cryogel for albumin depletion from human serum.* Journal of Molecular Recognition, 2012. **25**(11): p. 555-563.
19. Henderson, T.M., et al., *Cryogels for biomedical applications.* Journal of Materials Chemistry B, 2013. **1**(21): p. 2682-2695.
20. Jurga, M., et al., *The performance of laminin-containing cryogel scaffolds in neural tissue regeneration.* Biomaterials, 2011. **32**(13): p. 3423-3434.
21. Bloch, K., et al., *Functional activity of insulinoma cells (INS-1E) and pancreatic islets cultured in agarose cryogel sponges.* Journal of Biomedical Materials Research Part A: An Official Journal of The Society for Biomaterials, The Japanese Society for Biomaterials, and The Australian Society for Biomaterials and the Korean Society for Biomaterials, 2005. **75**(4): p. 802-809.

22. Singh, D., V. Nayak, and A. Kumar, *Proliferation of myoblast skeletal cells on three-dimensional supermacroporous cryogels.* International journal of biological sciences, 2010. **6**(4): p. 371.

23. Dainiak, M.B., et al., *Gelatin–fibrinogen cryogel dermal matrices for wound repair: preparation, optimisation and in vitro study.* Biomaterials, 2010. **31**(1): p. 67-76.

24. Takei, T., et al., *Synthesis of a chitosan derivative soluble at neutral pH and gellable by freeze–thawing, and its application in wound care.* Acta Biomaterialia, 2012. **8**(2): p. 686-693.

25. Shevchenko, R.V., et al., *The in vitro characterization of a gelatin scaffold, prepared by cryogelation and assessed in vivo as a dermal replacement in wound repair.* Acta biomaterialia, 2014. **10**(7): p. 3156-3166.

26. Berillo, D.A., et al., *A cryogel-based bioreactor for water treatment applications.* Water research, 2019. **153**: p. 324-334.

27. Ingavle, G.C., et al., *Affinity binding of antibodies to supermacroporous cryogel adsorbents with immobilized protein A for removal of anthrax toxin protective antigen.* Biomaterials, 2015. **50**: p. 140-153.

28. Jain, E., et al., *Fabrication of macroporous cryogels as potential hepatocyte carriers for bioartificial liver support.* Colloids and Surfaces B-Biointerfaces, 2015. **136**: p. 761-771.

29. Damania, A., et al., *Alleviating liver failure conditions using an integrated hybrid cryogel based cellular bioreactor as a bioartificial liver support.* Scientific Reports, 2017. **7**.

30. Damania, A., et al., *Decellularized liver matrix-modified cryogel scaffolds as potential hepatocyte carriers in bioartificial liver support systems and implantable liver constructs.* ACS applied materials & interfaces, 2018. **10**(1): p. 114-126.

31. Kan, P., et al., *Effects of shear stress on metabolic function of the co-culture system of hepatocyte/nonparenchymal cells for a bioartificial liver.* ASAIO journal (American Society for Artificial Internal Organs: 1992), 1998. **44**(5): p. M441-4.

32. Vinci, B., et al., *Modular bioreactor for primary human hepatocyte culture: medium flow stimulates expression and activity of detoxification genes.* Biotechnology journal, 2011. **6**(5): p. 554-564.

33. Esch, M.B., et al., *Multi-cellular 3D human primary liver cell culture elevates metabolic activity under fluidic flow.* Lab on a Chip, 2015. **15**(10): p. 2269-2277.

34. Powers, M.J., et al., *A microfabricated array bioreactor for perfused 3D liver culture.* Biotechnology and Bioengineering, 2002. **78**(3): p. 257-269.

35. Raimondi, M.T., et al., *Mechanobiology of engineered cartilage cultured under a quantified fluid-dynamic environment.* Biomechanics and modeling in mechanobiology, 2002. **1**(1): p. 69-82.

36. Zermatten, E., et al., *Micro-computed tomography based computational fluid dynamics for the determination of shear stresses in scaffolds within a perfusion bioreactor.* Annals of biomedical engineering, 2014. **42**(5): p. 1085-1094.

37. Cioffi, M., et al., *Modeling evaluation of the fluid-dynamic microenvironment in tissue-engineered constructs: A micro-CT based model.* Biotechnology and bioengineering, 2006. **93**(3): p. 500-510.

38. Chung, C., et al., *Enhancement of cell growth in tissue-engineering constructs under direct perfusion: Modeling and simulation.* Biotechnology and bioengineering, 2007. **97**(6): p. 1603-1616.

39. Martin, I., D. Wendt, and M. Heberer, *The role of bioreactors in tissue engineering.* Trends in Biotechnology, 2004. **22**(2): p. 80-86.

40. Marin, A.C., et al., *µ-Particle tracking velocimetry and computational fluid dynamics study of cell seeding within a 3D porous scaffold.* Journal of the mechanical behavior of biomedical materials, 2017. **75**: p. 463-469.

41. Adrian, R.J., *Twenty years of particle image velocimetry.* Experiments in fluids, 2005. **39**(2): p. 159-169.

42. Santiago, J.G., et al., *A particle image velocimetry system for microfluidics.* Experiments in fluids, 1998. **25**(4): p. 316-319.

43. Magin, C.M., S.P. Cooper, and A.B. Brennan, *Non-toxic antifouling strategies.* Materials Today, 2010. **13**(4): p. 36-44.

44. Ruoslahti, E. and M.D. Pierschbacher, *New perspectives in cell adhesion: RGD and integrins.* Science, 1987. **238**(4826): p. 491-497.

45. Hersel, U., C. Dahmen, and H. Kessler, *RGD modified polymers: biomaterials for stimulated cell adhesion and beyond.* Biomaterials, 2003. **24**(24): p. 4385-4415.

46. Merrifield, R.B., *Solid phase peptide synthesis. I. The synthesis of a tetrapeptide.* Journal of the American Chemical Society, 1963. **85**(14): p. 2149-2154.

47. Amblard, M., et al., *Methods and protocols of modern solid phase peptide synthesis.* Molecular biotechnology, 2006. **33**(3): p. 239-254.

48. Santini, M., M. Guilizzoni, and S. Fest-Santini, *X-ray computed microtomography for drop shape analysis and contact angle measurement.* Journal of colloid and interface science, 2013. **409**: p. 204-210.

49. Santini, M., S. Fest-Santini, and P. Foltyn, *On the local mass transfer rates around arbitrary shaped particles calculated by X-ray computed microtomography: Prospective for a novel experimental technique.* International Communications in Heat and Mass Transfer, 2016. **79**: p. 135-139.

50. Arvidsson, P., et al., *Chromatography of microbial cells using continuous supermacroporous affinity and ion-exchange columns.* Journal of Chromatography A, 2002. **977**(1): p. 27-38.

51. Thielicke, W. and E. Stamhuis, *PIVlab–towards user-friendly, affordable and accurate digital particle image velocimetry in MATLAB.* Journal of Open Research Software, 2014. **2**(1).

52. Harry, D., et al., *Increased sensitivity to endotoxemia in the bile duct–ligated cirrhotic rat.* Hepatology, 1999. **30**(5): p. 1198-1205.

53. Gómez-Ordóñez, E. and P. Rupérez, *FTIR-ATR spectroscopy as a tool for polysaccharide identification in edible brown and red seaweeds.* Food Hydrocolloids, 2011. **25**(6): p. 1514-1520.

54. Clayton, R.F., et al., *Liver cell lines for the study of hepatocyte functions and immunological response.* Liver International, 2005. **25**(2): p. 389-402.

55. Seal, B.L., T.C. Otero, and A. Panitch, *Polymeric biomaterials for tissue and organ regeneration.* Materials Science & Engineering R-Reports, 2001. **34**(4-5): p. 147-230.

56. Wood, B.D., X. He, and S.V. Apte, *Modeling turbulent flows in porous media.* Annual Review of Fluid Mechanics, 2020. **52**: p. 171-203.

57. Balasubramaniyan, V., et al., *Ammonia reduction with ornithine phenylacetate restores brain eNOS activity via the DDAH-ADMA pathway in bile duct-ligated cirrhotic rats.* American Journal of Physiology-Gastrointestinal and Liver Physiology, 2012. **302**(1): p. G145-G152.

58. Shah, N., et al., *Prevention of acute kidney injury in a rodent model of cirrhosis following selective gut decontamination is associated with reduced renal TLR4 expression.* Journal of hepatology, 2012. **56**(5): p. 1047-1053.

59. Kountouras, J., B.H. Billing, and P.J. Scheuer, *Prolonged bile duct obstruction: a new experimental model for cirrhosis in the rat.* British journal of experimental pathology, 1984. **65**(3): p. 305.